Millennial-scale hydroclimate control of tropical soil carbon storage

https://doi.org/10.1038/s41586-020-2233-9

Received: 5 September 2018

Accepted: 17 February 2020

Published online: 6 May 2020



Check for updates

Christopher J. Hein^{1⊠}, Muhammed Usman^{2,3}, Timothy I. Eglinton², Negar Haghipour^{2,4} & Valier V. Galv5

The storage of organic carbon in the terrestrial biosphere directly affects atmospheric concentrations of carbon dioxide over a wide range of timescales. Within the terrestrial biosphere, the magnitude of carbon storage can vary in response to environmental perturbations such as changing temperature or hydroclimate¹, potentially generating feedback on the atmospheric inventory of carbon dioxide. Although temperature controls the storage of soil organic carbon at mid and high latitudes^{2,3}, hydroclimate may be the dominant driver of soil carbon persistence in the tropics^{4,5}; however, the sensitivity of tropical soil carbon turnover to large-scale hydroclimate variability remains poorly understood. Here we show that changes in Indian Summer Monsoon rainfall have controlled the residence time of soil carbon in the Ganges-Brahmaputra basin over the past 18,000 years. Comparison of radiocarbon ages of bulk organic carbon and terrestrial higher-plant biomarkers with co-located palaeohydrological records⁶ reveals a negative relationship between monsoon rainfall and soil organic carbon stocks on a millennial timescale. Across the deglaciation period, a depletion of basin-wide soil carbon stocks was triggered by increasing rainfall and associated enhanced soil respiration rates. Our results suggest that future hydroclimate changes in tropical regions are likely to accelerate soil carbon destabilization, further increasing atmospheric carbon dioxide concentrations.

The size of the atmospheric CO₂ reservoir (around 750 Pg C at present) is modulated in part by exchanges with active reservoirs of biospheric organic carbon (BOC), such as marine primary producers, dissolved organic carbon, terrestrial vegetation and soils. Of these, the terrestrial carbon cycle remains the least well constrained, reflecting the complexity of terrestrial ecosystem sensitivity to changes in atmospheric temperature^{8,9}, CO₂ concentrations¹⁰, nutrient availability¹¹ and hydroclimate⁴. In particular, the sensitivity of soil carbon stocks (with a global reservoir of 1,600 Pg C) to climate remains unresolved, hindering projections of carbon cycling under future climate-change scenarios. Soil carbon storage is a function of inputs from leaf and root detritus associated with net primary productivity; and outputs through lateral export via rivers, CO₂ and CH₄ efflux due to root respiration and microbial decomposition, and fire emissions¹. Soil carbon respiration rates and thus turnover times—respond directly to temperature changes^{2,3}. However, recent findings have revealed that this effect is muted in the tropics, where hydroclimate variability may have a more important role in climate/carbon-cycle feedback^{4,5}. To test this hypothesis, we reconstruct how hydroclimate change since the Late Glacial period (24–18 ka) has affected the dynamics of soil organic carbon cycling in a continent-sized tropical basin. Specifically, we determine the mean age of terrestrial BOC-a proxy for the dynamics of the soil carbon reservoir-eroded from the Ganges-Brahmaputra river basin and stored in Bengal Fan sediments. We then compare temporal variations in this mean age with variations in the intensity of the Indian Summer Monsoon (ISM) to reveal the sensitivity of tropical soil carbon stocks to changing hydroclimate.

Post-glacial climate proxy records

Rivers integrate sediments, organic matter and dissolved constituents from across their drainage basins, allowing downstream archives to capture basin-scale changes in, for example, environmental conditions, sediment fluxes and organic carbon cycling¹². The radiocarbon (¹⁴C) content of BOC laterally exported with river sediments provides an estimate of the integrated mean age of BOC in the basin, and, as such, can be used as a proxy for the dynamics of terrestrial organic carbon cycling. Riverine particulate organic carbon is, however, known to be highly heterogeneous¹³: it may include ¹⁴C-free petrogenic carbon derived from rock erosion^{14,15} and BOC that is a mixture of fresh organic matter derived from, for example, aquatic productivity and leaf litter, as well as organic matter that is 'pre-aged'-that is, stored in soils and floodplain deposits before export (for example, see ref. 16). As such, in addition to bulk organic carbon, we use compound-specific ¹⁴C dating of molecular biomarkers specifically produced by terrestrial vascular plants: long-chain leaf-wax n-alkanoic acids (C_{24-34} fatty acids).

Department of Physical Sciences, Virginia Institute of Marine Science, William & Mary, Gloucester Point, VA, USA, 2Geological Institute, Department of Earth Sciences, ETH, Zurich, Switzerland, ³Department of Physical & Environmental Sciences, University of Toronto Scarborough, Toronto, Ontario, Canada. ⁴Laboratory for Ion Beam Physics, Department of Physics, ETH, Zurich, Switzerland. 5Department of Marine Chemistry and Geochemistry, Woods Hole Oceanographic Institution, Woods Hole, MA, USA. E-mail: hein@vims.edu

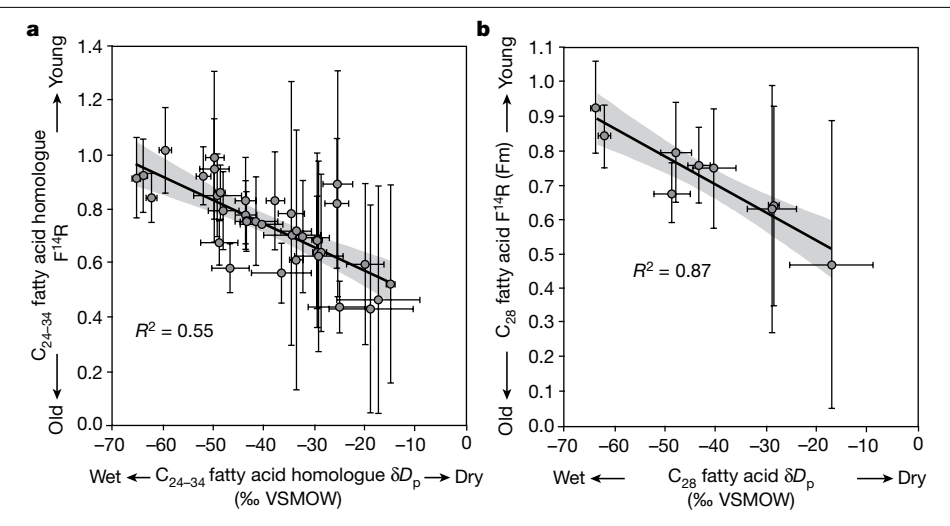


Fig. 1| **Correlation between palaeoclimate proxies with organic-matter age structure. a, b,** Post-glacial precipitation δD_P values, derived from ice-volume-and vegetation-fractionation-corrected fatty acid δD values (see ref. ⁶ and Methods for details), are plotted against the degree of pre-ageing of organic matter (given as $F^{14}R$, in dimensionless units). **a,** $F^{14}R$ values (n=35) of individual

homologues of C_{24-34} fatty acids plotted against δD_P values of those same C_{24-34} fatty acids. **b**, $F^{14}R$ values (n=9) of C_{28} fatty acids versus δD_P values of those same C_{28} fatty acids. Error bars indicate propagated measurement ($F^{14}R$) or standard deviation (δD_P) errors. VSMOW, Vienna standard mean ocean water; R^2 , coefficient of determination.

To reconstruct variability in soil-carbon storage dynamics within the Ganges–Brahmaputra basin following the Late Glacial, we couple $^{14}\mathrm{C}$ dating of bulk organic carbon and C_{24-34} fatty acids in fine-grained turbidite beds from a suite of three gravity piston cores collected in the Bengal Fan channel-levee system (see Methods and Extended Data Fig. 1). These cores record basin-scale hydroclimate and vegetation change over a roughly 18,000-year period (Supplementary Table 1 and Extended Data Fig. 2), notably an order-of-magnitude shift in the strength of the ISM between the Late Glacial/Heinrich Stadial 1 (HS1; 18–15 ka) and the Holocene Climatic Optimum (HCO; 10.0–6.5 ka) 6 . Combining these palaeoenvironmental signatures with time-varying lipid age structures from this same suite of biomarkers allows us to quantify the sensitivity of soil-carbon storage within this tropical drainage basin to changing hydroclimatic conditions over millennial timescales.

Climatic control of organic carbon age structure

Values for the fraction modern (Fm) of bulk organic carbon (see Methods: n = 89) range from 0.085 to 0.648 (Supplementary Table 2). Applying a constant 3% relative contribution of petrogenic organic carbon (following modern values¹⁷; see Methods), we calculate Fm values for bulk BOC of 0.089-0.683. This large range primarily reflects deposition spanning nearly the past 18,000 years: corrected for deposition age, the radiocarbon age of bulk BOC since the Late Glacial at the time of delivery to the Bengal Fan (its 'reservoir offset' value; see Methods and ref. 18) ranged between around 1,300 and 5,850 14C years (Supplementary Table 2). The mean bulk BOC reservoir offset-3,250 ¹⁴C years-is nearly identical to those determined for modern Ganges-Brahmaputra river BOC¹⁷. C₂₈ and weighted-average C₂₄₋₃₂ fatty acid homologues have reservoir offset values of around 640-6,150 ¹⁴C years (average 2,790 ¹⁴C years) and approximately 375-6,000 ¹⁴C years (average 2,672 ¹⁴C years), respectively (Supplementary Table 3 and Extended Data Fig. 3a). We find relatively close agreement between bulk BOC and corresponding C₂₈ and C₂₄₋₃₂ fatty acid reservoir offset values; however, bulk BOC for a given sample is systematically more pre-aged (that is, older at the time of export owing to storage on land) than are corresponding long-chain fatty acids (Extended Data Fig. 3b), reflecting the contribution of more diverse, and older, organic matter to the bulk biospheric pool¹⁷.

Characterized in terms of 'reservoir relative enrichment' (F¹⁴R; see Methods and ref. ¹⁸), the age structures of our bulk BOC and fatty

acids are closely correlated with the hydrogen stable-isotope composition of precipitation (δD_P) determined from the same compounds¹⁹ (Fig. 1 and Extended Data Fig. 3); weaker correlations with bulk BOC (Extended Data Fig. 4a) probably reflect more heterogeneous source inputs contributing to bulk organic carbon. We can further refine our organic carbon age estimates by taking advantage of the results of ref. 19, in which numerical modelling was applied to 14C signatures of biomarkers from a sediment core collected from the head of the Bengal Fan channel-levee system, which captures the past 70 years of sediment deposition and was used to estimate the timescales of BOC storage within the modern watershed. They divide the pool of C_{24-34} fatty acids into 'fast' (for example, leaf litter) and 'slow' (for example, mineral soil organic carbon) cycling components. These contribute fatty acids cycled on decadal (average age 15 calendar years) and centennial to millennial (average age 1,000-1,200 calendar years) timescales, respectively; the latter constitute 79-83% of the long-chain fatty acid pool. Assuming that fresh, decadal (roughly 15-year cycling time) BOC has always contributed to the Ganges-Brahmaputra rivers from vegetation debris and soil litter at rates similar to today's (see Methods), we calculate millennial bulk BOC and biomarker ages for the past 18 kyr. We find that, following deglaciation, both closely track—with an apparent lag of roughly 1,000 years-hydroclimate shifts determined from both these same Bengal Fan channel-levee cores and independent records (Fig. 2).

Together, these results indicate that variations in monsoon strength led directly to changes in terrestrial BOC mean age since the Late Glacial. Using C_{28} fatty acids, for which correlation is the most robust, we find that a 10% shift in δD_P values corresponds to a roughly 0.1 change in millennial $F^{14}R$. This represents, for example, a change in bulk BOC mean age of 2,600 ^{14}C years between HS1 and the HCO, corresponding to a decrease in terrestrial BOC storage times of more than 50%. Given the concurrent transition of terrestrial vegetation from dominantly C4 (savanna-like) to dominantly C3 (forest-like)⁶, which would probably increase overall soil carbon storage capacity, this change in BOC storage time suggests a direct, positive influence of the warmer and wetter conditions within the Ganges–Brahmaputra basin on soil carbon turnover rates.

Given modern-system age distributions ¹⁹, it is not possible to produce $C_{28}F^{14}R$ values of less than about 0.80, even by increasing the contribution of the millennial BOC component to 100%. Thus, the only means by which to achieve the $F^{14}R$ values observed throughout the deglacial

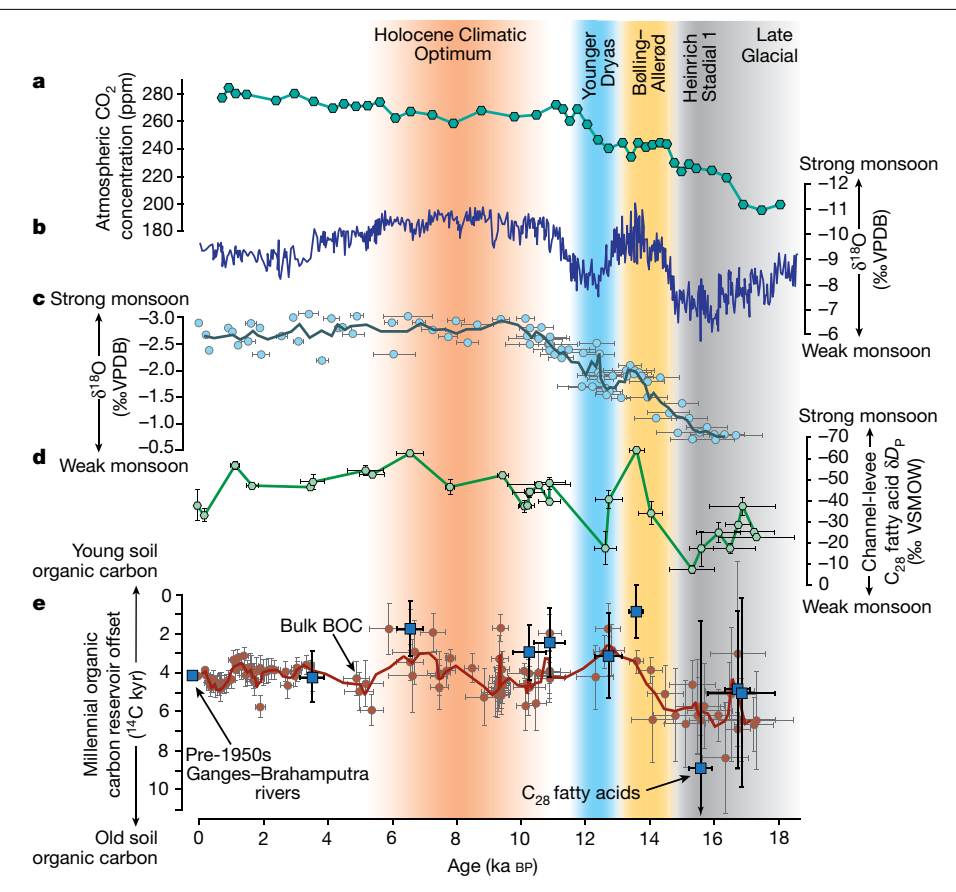


Fig. 2 | Temporal variations in climate forcings and soil organic-carbon storage. a-e, Comparison of: post-glacial wet-extraction atmospheric CO₂ concentrations from Dome Fuji Ice Core³⁰ using the gas-age profile (a): ISM strength as given by a composite Chinese cave speleothem δ^{18} O record³¹ (**b**), by δ^{18} O of planktonic foraminifers (Globigerinoides ruber) (n = 81) (**c**) and calculated as precipitation δD_p from terrestrial biomarker δD from the Bengal Fan channel-levee (n = 30) (d); and records of the age structure of bulk biospheric organic carbon (red circles; n = 116) and biomarkers (C_{28} fatty acids; blue squares; n = 9) exported from the Ganges-Brahmaputra basin (e). Data in

 ${f c}$, ${f d}$ are replotted from ref. 6) with our updated core age-depth model. Data in e are given as the difference between the age of the millennial component of biomarkers/bulk BOC and the deposition age (in ¹⁴C vrs). Solid lines in **c**. **e** are three-point moving averages. Pre-1950s Ganges-Brahmaputra river data in e are from ref. 19. Vertical error bars indicate propagated measurement uncertainties (reservoir offset values) or multimeasurement standard deviation (8D) errors for instrumental measurements; horizontal error bars in **c-e** are core age-model deposition-age error estimates (see Methods).

and Holocene period is to increase the age of the millennial component of BOC. This is supported by the high abundance of fatty acids during warm, wet periods (Extended Data Fig. 5) and by moderate correlations between fatty-acid abundance and each bulk and biomarker F14R (Extended Data Fig. 6). This reflects the export of biomarker-lean (that is, degraded), old BOC during cooler, drier periods, and implies that our Late Glacial and HS1 millennial BOC age estimates are conservative: given any contribution of decadal BOC during these periods (that is, a decadal-to-millennial BOC ratio of more than 0), then an even older millennial BOC contribution is required to produce such low BOC F¹⁴R values. Our data thus indicate enhanced (with respect to modern) pre-ageing of BOC within the Ganges-Brahmaputra basin during the cooler, drier periods associated with a weak ISM. The subsequent post-Late Glacial and pre-HCO decreases in the age of the millennial component of the BOC delivered to the Bengal Fan correspond directly to warming and moistening of the basin (Fig. 2).

Implications for the global carbon cycle

The old apparent age of BOC laterally exported to the Bengal Fan suggests that the modern Ganges-Brahmaputra basin stores and exports large quantities of BOC that accumulated over centuries to millennia¹⁹. Basin-wide, climate-driven changes in this post-deglaciation age structure track not soil carbon provenance (see Methods), but rather the residence time of that soil carbon within the terrestrial environment, at least over millennial timescales. Thus, the decrease in millennial BOC mean age from the Late Glacial to post-HS1 periods (Fig. 2e) corresponds to an acceleration in soil carbon turnover (a decreasing mean age) by a factor of nearly two. This would have resulted from enhanced soil organic carbon respiration, providing a positive feedback on atmospheric CO₂ concentrations, with a partial reversal in recent millennia following the HCO.

Considering only the post-Late Glacial period reveals another feature of the observed soil carbon-climate feedback. Given that BOC delivered to the coastal ocean represents only around 3% of total annual soil-carbon turnover within the modern Ganges-Brahmaputra basin (the remaining 97% is attributed to CO₂ fluxes to the atmosphere through heterotrophic respiration and fires⁵), accounting for the observed 4,100 ¹⁴C-year change in millennial BOC age through lateral carbon fluxes (erosion and fluvial export) between HS1 and the Bølling-Allerød, without a commensurate increase in soil respiration fluxes, would require a nearly twofold increase in lateral BOC fluxes. This same change requires only a 7.5% increase in soil respiration fluxes (see Methods). Although our data do not allow us to distinguish between these mechanisms, the dependence of soil organic carbon turnover on hydroclimate is best explained by an imbalance between increasing organic carbon heterotrophic respiration and net primary productivity. The observed 1,000-year lag in millennial reservoir offset

values as compared with hydroclimate proxy records (Fig. 2) probably represents the system response time; an instantaneous shift in soil turnover will take centuries to shift the overall age structure of soil carbon and associated laterally exported organic carbon. Moreover, correlations are much weaker between the millennial age structure of organic carbon and atmospheric CO₂ concentrations (Fig. 2a) than with direct measures of hydroclimate (Fig. 2b-d). This suggests that soil fertilization (increase in productivity related to increasing CO₂) may not exert a first-order control on soil organic carbon turnover, but rather is filtered through the (hydro)climate system. This implies that, in the tropics, the climate/carbon-cycle feedback is not simple and one-directional, but rather is responsive to the impact of CO₂-associated warming on terrestrial precipitation patterns, confirming at the millennial scale, and in a globally important system, observations from subdecadal-scale arid-climate macrocosm experiments²⁰.

The Ganges-Brahmaputra rivers are globally important in terms of sediment load $(1-2 \times 10^9 \text{ t yr}^{-1}; \text{ ref.}^{-21})$, carbon burial (roughly 4.7×10^{12} g yr⁻¹, around 20% of the global terrestrial BOC burial flux; refs. ^{22,23}), and marine sequestration of terrigenous organic carbon at timescales of thousands to millions of years 6,22,24. Our results demonstrate that warmer, wetter conditions associated with post-glacial strengthening of the ISM led to release of pre-aged BOC from within this basin. Although it is not clear that increased atmospheric CO₂ concentrations (and associated climatic warming) directly lead to increased ISM rainfall intensity²⁵, we find an apparent positive feedback between hydroclimate and atmospheric CO₂ concentrations, acting through changes in the soil carbon stock over millennial timescales, most likely triggered by enhanced heterotrophic respiration. In this manner, we find a low-latitude climate feedback similar to that reported for high-latitude permafrost soils²⁶. This supports findings from carbon-cycle models of glacial gross primary productivity and terrestrial carbon stocks, which suggest overall turnover times and associated large 'inert' terrestrial carbon stocks (in soils, permafrost and wetlands) nearly doubled during the last glacial period²⁷. Our study reveals that tropical soils may have contributed substantially to this glacial 'inert' terrestrial carbon pool—previously attributed nearly exclusively to permafrost²⁷. Our results further show that future hydroclimate change—in which decreases in the strength of the ISM are likely to be more than compensated by increased atmospheric moisture content, leading to more overall precipitation^{28,29}—is likely to further accelerate soil organic carbon destabilization (turnover rates and/or net loss of carbon stocks) in the tropics, increasing atmospheric BOC fluxes through enhanced soil decomposition or transport-induced oxidation, and thus further increasing atmospheric CO₂ concentrations.

Online content

Any methods, additional references, Nature Research reporting summaries, source data, extended data, supplementary information, acknowledgements, peer review information; details of author contributions and competing interests; and statements of data and code availability are available at https://doi.org/10.1038/s41586-020-2233-9.

Davidson, E. A. & Janssens, I. A. Temperature sensitivity of soil carbon decomposition and feedbacks to climate change, Nature 440, 165-173 (2006).

- Melillo, J. M. et al. Soil warming and carbon-cycle feedbacks to the climate system. Science 298, 2173-2176 (2002).
- Lloyd, J. & Taylor, J. A. On the temperature dependence of soil respiration. Funct. Ecol. 8, 315-323 (1994).
- Carvalhais, N. et al. Global covariation of carbon turnover times with climate in terrestrial ecosystems, Nature 514, 213-217 (2014).
- Bloom, A. A., Exbrayat, J. F., van der Velde, I. R., Feng, L. & Williams, M. The decadal state of the terrestrial carbon cycle: global retrievals of terrestrial carbon allocation, pools, and residence times. Proc. Natl Acad. Sci. USA 113, 1285-1290 (2016).
- Hein, C. J., Galy, V. V., Galy, A., France-Lanord, C. & Kudrass, H. Post-glacial climate forcing of surface processes in the Ganges-Brahmaputra river basin and implications for carbon sequestration. Earth Planet. Sci. Lett. 478, 89-101 (2017).
- Friend, A. D. et al. Carbon residence time dominates uncertainty in terrestrial vegetation responses to future climate and atmospheric CO₂, Proc. Natl Acad. Sci. USA 111, 3280-3285 (2014).
- Xia. J. et al. Terrestrial carbon cycle affected by non-uniform climate warming. Nat Geosci. 7. 173-180 (2014).
- Hicks Pries, C. E. H., Castanha, C., Porras, R. C. & Torn, M. S. The whole-soil carbon flux in response to warming, Science 355, 1420-1423 (2017).
- Schimel, D., Stephens, B. B. & Fisher, J. B. Effect of increasing CO₂ on the terrestrial carbon cycle. Proc. Natl Acad. Sci. USA 112, 436-441 (2015)
- Wieder, W. R., Cleveland, C. C., Smith, W. K. & Todd-Brown, K. Future productivity and carbon storage limited by terrestrial nutrient availability. Nat. Geosci. 8, 441-444 (2015).
- Simpson, G. & Castelltort, S. Model shows that rivers transmit high-frequency climate cycles to the sedimentary record. Geology 40, 1131-1134 (2012).
- Aufdenkampe, A. K. et al. Organic matter in the Peruvian headwaters of the Amazon: compositional evolution from the Andes to the lowland Amazon mainstem. Org. Geochem, 38, 337-364 (2007)
- Drenzek, N. et al. A new look at old carbon in active margin sediments. Geology 37, 239-242 (2009)
- Hilton, R. G., Galy, A., Hovius, N. & Horng, M. J. Efficient transport of fossil organic carbon to the ocean by steep mountain rivers: an orogenic carbon sequestration mechanism. Geology 39, 71-74 (2011).
- Schefuß, E. et al. Hydrologic control of carbon cycling and aged carbon discharge in the Congo River basin. Nat. Geosci. 9, 687-690 (2016).
- Galy, V. & Eglinton, T. I. Protracted storage of biospheric carbon in the Ganges-Brahmaputra basin. Nat. Geosci. 4, 843-847 (2011).
- Soulet, G., Skinner, L. C., Beaupré, S. R. & Galv, V. A note on reporting of reservoir 14C disequilibria and age offsets. Radiocarbon 58, 205-211 (2016).
- French, K. L. et al. Millennial soil retention of terrestrial organic carbon matter deposited in the Bengal Fan. Sci. Rep. 8, 11997 (2018).
- Yu. H. et al. Soil carbon release responses to long-term versus short-term climatic warming in an arid ecosystem. Biogeosci. 17, 781-792 (2020).
- Milliman, LD, & Syvitski, LP, Geomorphic/tectonic control of sediment discharge to the ocean: the importance of small mountainous rivers, J. Geol. 100, 525-544 (1992).
- Galy, V. et al. Efficient organic carbon burial in the Bengal fan sustained by the Himalayan erosional system. Nature 450, 407-410 (2007).
- Galy, V., Peucker-Ehrenbrink, B. & Eglinton, T. Global carbon export from the terrestrial biosphere controlled by erosion. Nature 521, 204-207 (2015).
- France-Lanord, C. & Derry, L. A. Organic carbon burial forcing of the carbon cycle from Himalayan erosion. Nature 390, 65-67 (1997).
- Roxy, M. K. et al. Drying of Indian subcontinent by rapid Indian Ocean warming and a weakening land-sea thermal gradient. Nat. Commun. 6, 7423 (2015).
- Gustafsson, Ö., Van Dongen, B. E., Vonk, J. E., Dudarev, O. V. & Semiletov, I. P. Widespread release of old carbon across the Siberian Arctic echoed by its large rivers. Biogeosciences 8, 1737-1743 (2011).
- Ciais, P. et al. Large inert carbon pool in the terrestrial biosphere during the Last Glacial Maximum. Nat. Geosci. 5, 74-79 (2012).
- Christensen, J. H. et al. in Climate Change 2013: The Physical Science Basis. Contribution of Working Group I to the Fifth Assessment Report of the Intergovernmental Panel on Climate Change (eds Stocker, T. F. et al.) 1217-1308 (Cambridge University Press, 2013)
- Sharmila, S., Joseph, S., Sahai, A. K., Abhilash, S. & Chattopadhyay, R. Future projection of Indian summer monsoon variability under climate change scenario: an assessment from CMIP5 climate models. Global Planet. Change 124, 62-78 (2015).
- Kawamura, K. et al. Northern Hemisphere forcing of climatic cycles in Antarctica over the past 360,000 years, Nature 448, 912-916 (2007).
- Cheng, H. et al. The Asian monsoon over the past 640,000 years and ice age terminations. Nature 534, 640-646 (2016); corrigendum 541, 122 (2016)

Publisher's note Springer Nature remains neutral with regard to jurisdictional claims in published maps and institutional affiliations.

© The Author(s), under exclusive licence to Springer Nature Limited 2020

Methods

Sediment cores

Three gravity piston cores were retrieved at water depths of 2,540-2.610 m along the middle fan channel-levee system (inner-levee. outer-levee, and levee-proximal) during the February 1994 (Expedition SO93) cruise of the R/V SONNE³², coincident with sediment echosounder data (Extended Data Fig. 1; see ref. 6 and its associated supplementary information for details). Sediment core age models are updated from ref. 6 and based on a recalibration of 22 reported 6,32 radiocarbon (14C) ages derived from planktonic foraminifera (Globigerinoides sacculifer and Globigerinoides ruber) and accelerator mass spectrometry (AMS) radiocarbon dating of planktonic G. ruber from an additional four sedimentary units within core SO93-118KL (Supplementary Table 1). Radiocarbon ages were calibrated using OxCal 4.2 (ref. 33) with the IntCal13 curve34 and a regionally averaged marine reservoir correction (ΔR) of -4 ± 42 years (data from refs. ^{35,36}). Age models were calculated in the age-depth modelling software package Clam 2.1 (ref. ³⁷) with extrapolation to core bottoms (Extended Data Fig. 2). Together, these capture the last 17.5 kyr of deposition, with linearized sediment accumulation rates of less than 50 cm kyr⁻¹ to more than 500 cm kyr⁻¹ (see ref. ⁶ for details).

Bulk organic carbon radiocarbon analysis

Following fumigation acidification, radiocarbon analysis was completed on powdered bulk-sediment aliquots from 89 samples (each representing 1–10 cm thick core sections). Samples were fumigated by sealing in a vacuum desiccator with a beaker of 50 ml 12N HCl, exposed to HCl fumes for 60–72 h at 60–65 °C to remove carbonates, and dried in a separate desiccator for an additional 24 h. Radiocarbon analyses were conducted at either the National Ocean Science Accelerator Mass Spectrometry (NOSAMS) facility (Woods Hole, MA) or with the ETH Zurich AMS 'MICADAS' system (see ref. 38 for details). Detailed results are provided in Supplementary Table 2.

Compound-specific radiocarbon analysis

Fatty acids derived from lipid extracts from a subset of nine samples were purified by aminopropyl-silica-gel column chromatography, derivatized with methanol of known isotopic composition to produce fatty acid methyl esters (FAMEs), and then further purified by aminopropyl-silica-gel chromatography and silver nitrate-silica-gel chromatography (see ref. 6 for details). Six individual, saturated, long-chain FAMEs (n- C_{24} , n- C_{26} , n- C_{30} , n- C_{32} and n- C_{34}) were purified and collected according to the preparative capillary gas chromatography (PCGC) method^{17,39}. This was done through a suite of up to 100, 3-5 µl injections of a saturated FAME solution in iso-octane (individual homologues at 50-200 ng µl⁻¹ concentrations) on either an Agilent 7890A or an HP 5890 Series II gas chromatograph (GC) coupled to a Gerstel preparative fraction collector (PFC). PCGC traps were recovered with 4 ml of DCM and further purified to remove column bleed by 1% deactivated silica-gel column chromatography, using around 3 cm of gel and eluting FAME homologues in 4 ml of DCM. Homologue purity was checked by injecting a small aliquot on a GC-flame ionization detector (FID), and yields were determined to a range between around 40% and 80%. To increase sample size and reduce analytical uncertainty during radiocarbon analyses, it was necessary to combine homologues following isolation by PCGC for two samples: (1) for sample SO93-120KL 1,130-1,140 cm, two sets of homologues were combined: n-C₂₄ and n-C₂₆ (treated as a C₂₄ sample for purposes of data analysis) and n-C $_{28}$, n-C $_{30}$ and n-C $_{32}$ (treated as a C $_{28}$ sample); and (2) for sample SO93-120KL 632-642 cm, n- C_{32} and n- C_{34} homologues were combined (treated as a C_{32} sample).

PCGC-purified FAME homologues were dissolved in DCM and loaded into premuffled quartz tubes. Solvent was evaporated under a high-purity nitrogen stream and combusted copper oxide (roughly

150 µg) was added to the quartz tube. Quartz tubes were evacuated to less than 30 µTorr and flame-sealed on a vacuum line following chilling using dry ice/isopropanol slurry and liquid nitrogen cryogenic traps to prevent sublimation of FAMEs. Samples were combusted in flame-sealed quartz tubes at 850 °C for 5 h, and, the following day, were cracked under vacuum; the released CO_2 was cryogenically purified and manometrically quantified. The sample CO_2 was trapped using liquid nitrogen, flame-sealed in a pyrex tube, and sent to either ETH Zurich or NOSAMS where they were analysed for ¹⁴C content as a gas target with the Micadas gas ion source as described ³⁸ (ETH Zurich), or as a graphite target following catalytic conversion as described ^{40,41} (NOSAMS).

Resulting ¹⁴C measurements were corrected for procedural blanks (the blank correction varies among the samples, depending on the mass of the measured fractions; see Supplementary Table 3), and for the addition of derivative carbon during methylation with MeOH with a known ¹⁴C composition, using mass-balance equations (see ref. ¹⁹ for details).

A total of 40 14 C measurements were made on homologues (or combined homologues) from the 9 samples selected for analysis. Not all homologues were measured from all samples owing to insufficient compound availability or loss during sample preparation (for example, shattering of quartz tubes). Radiocarbon data are expressed as the fraction of modern carbon, Fm, precorrected for mass-dependent fractionation using the 13 C/ 12 C ratio measured online.

We observed relatively small differences in stable-isotope $(\delta D)^6$ and radioisotope (Extended Data Fig. 3a and Supplementary Table 3) compositions among C_{24-34} fatty acid homologues. Fatty acids generally, although not universally, become more 14 C-depleted with increasing chain length, a phenomenon commonly associated with the selective preservation of long-chain homologues 42,43 . C_{28} fatty acids—which were consistently the most abundant homologue (average concentration 0.64 μ g g $^{-1}$) and yielded the highest average C mass for 14 C analysis (48.8 μ g)—and weighted-average C_{24-32} fatty acids are the focus of discussion.

¹⁴C deposition ages

Sediment deposition ages (in ¹⁴C years) are determined from ¹⁴C analysis of planktonic foraminifera (*G. sacculifer* and *G. ruber*; Supplementary Table 1), corrected for a standard 400-year surface ocean ¹⁴C reservoir age offset. Deposition of 15 of our 118 samples is directly dated; the remaining deposition ages (with errors) are calculated through interpolation from ¹⁴C age-depth models constructed in the Clam 2.1 software package³⁷.

Radiocarbon terminology, conventions and calculations

Sample ¹⁴C contents are given in the nondimensional 'fraction modern' (Fm) notation—a measurement of the deviation of a sample ¹⁴C/¹²C ratio from 95% of the radiocarbon concentration at 'modern' (1950 CE) of NBS oxalic acid I (SRM 4990B, OX-I), normalized to a $\delta^{13}C_{VPDB}$ value of –19‰ (see refs. ^{44–46}). Given that Fm is a measure of the $^{14}C/^{12}C$ ratio, it is, by definition, a measure of the radiocarbon content of a sample, and can thus be related to the radiocarbon (uncalibrated) age of the sample as follows:

14
C age = $-8033 \times ln(Fm)$

Here, we seek to determine the amount of 'pre-aging' that organic matter has undergone before export and delivery to the coastal ocean, as a means of estimating soil organic carbon turnover rates. To accomplish this, we use the 'reservoir offset' metric, defined¹⁸ as a measure of the radiocarbon age offset, in ¹⁴C years, between two contemporaneous carbon reservoirs. This metric relies on the 'relative enrichment' of the reservoir, defined¹⁸ as the ratio of Fm values from two contemporaneous carbon reservoirs (*x* and *y*) at a given time (in our case, the time of deposition in the Bengal Fan). It is thus a measure of the age

(in ¹⁴C years) of organic matter at the time of its deposition. Relative enrichment is given by the notation F¹⁴R in dimensionless units, as follows:

$$F^{14}R_{x-y} = \frac{Fm_x}{Fm_y}$$

By convention, $F^{14}R$ is dimensionless and ranges from 0 to 1 by placing the more commonly enriched reservoir (y) in the denominator. From this, the reservoir age offset (R_{x-y}) can be determined:

$$R_{x-y} = -8033 \times \ln(F^{14}R_{x-y})$$

In order to calculate reservoir age offset values through time, it is necessary to 'uncalibrate' organic-matter deposition ages derived from the core-age models (derived from calibrated ¹⁴C ages of foraminifera, and plotted in calibrated (or 'calendar') years before present (BP), where 'present' is set by convention to the year 1950 CE). For this, we take advantage of the Bayesian 'uncalibration-convolution process' approach of ref. 47, which propagates uncertainties linked to the reservoir-derived ^{14}C age (in this case, bulk organic matter or biomarker Fm values), a weakly a priori known calendar age (in this case, derived from core-age models), and the atmospheric calibration curve (from IntCal13; ref. 34). Specifically, we apply to our biomarker, bulk organic carbon, and bulk biospheric organic carbon ages the radcal script of the ResAge Package⁴⁷, designed for pairs of reservoir-derived radiocarbon ages and a corresponding weakly known (with some uncertainty) calendar ages. This program uncalibrates age-model-derived deposition ages (that is, it converts these to 14C years) and calculates reservoir offset and F14R values for each input.

Determination of millennial BOC ages

 $F^{14}R$ values for each bulk and fatty acid homologue sample can be expressed as a function of the age (in Fm) of each the millennial (mil) and decadal (dec) pools, multiplied by the fractional contribution of each of those pools.

We hold the contributions to the overall Ganges-Brahmaputra organic-carbon pool of each of the decadal BOC (F_{dec}) , millennial BOC (F_{mil}) , and petrogenic organic carbon (F_{rxc}) constant through time. Specifically, petrogenic carbon is assumed to contribute 3% of all organic carbon to the bulk carbon pool (BOC is roughly 97% of total organic carbon), whereas fatty acids are free of petrogenic carbon (BOC roughly 100%); this assumption is founded in analyses of each river and Bengal Fan core-top sediments, which reveal that Ganges-Brahmaputra river sediments delivered to the Bay of Bengal at present contain roughly 0.03% petrogenic organic carbon^{17,48,49}. In addition, structural characterization (Raman and high-resolution transmission electron microscopy) of petrogenic organic carbon in sediments from the Bengal Fan dating back to the Miocene⁴⁸, coupled with evidence⁶ for high burial efficiency of terrestrial organic carbon over the past 20,000 years, suggests that the petrogenic organic-carbon concentration in Bengal Fan sediments has remained constant since the Last Glacial. Finally, we would anticipate that, if petrogenic contributions changed in any systematic manner through time, it would be reflected in bulk total organic carbon (TOC) values; indeed, bulk TOC shows no correlation either with the relative enrichment of bulk organic-carbon radiocarbon ($R^2 = 0.0036$; Extended Data Fig. 7a), or with petrogenic-contribution-corrected BOC relative enrichment ($R^2 = 0.0025$) or millennial BOC relative enrichment ($R^2 = 0.0024$).

Given these constraints, we apply time-invariant millennial and decadal contributions to BOC of 80% and 20%, respectively (values for modern Ganges–Brahmaputra rivers are from ref. 19). The fatty-acid decadal pool is assumed to always turnover quickly (by definition), and is assigned a constant 15-year cycling time ($F^{14}R = 0.9981$) 19 . The ^{14}C age of the millennial BOC is calculated at each time step as follows:

$$F^{14}R_{tot} = F^{14}R_{mil} \times F_{mil} + F^{14}R_{dec} \times F_{dec} + F^{14}R_{rxC} \times F_{rxC}$$

Constraining grain-size and palaeovegetation effects

Sediment organic-carbon concentrations are highly sensitive to sediment grain size, which, within the Ganges–Brahmaputra rivers and Bengal Fan, shows close correspondence with the production of aluminosilicate clays, and thus sediment Al/Si content 6,22,48,50 . However, neither the grain size (Al/Si) nor the grain-size-normalized TOC values of the Bengal Fan channel-levee cores show any discernible trend through time 6 . Further, we find no correlation between organic-matter age with respect to deposition time (that is, F 14 R values) and either TOC or Al/Si values (Extended Data Fig. 7).

Changes in vegetation since the Last Glacial were documented in ref. 6 using bulk and biomarker δ^{13} C values from the same cores used here. These changes were accounted for in ref. 6 in the development of the biomarker δD_p record (derived from the lipid δD record); we directly used those same biomarker-derived δD_p values here: a subset is presented in each of Fig. 1 and Extended Data Fig. 4, and the full δD_p record (that is, lipid δD values corrected for ice volume and palaeovegetation (from lipid δ^{13} C values)) is given in in Fig. 2.

Corrections of lipid δD values for ice-volume and lipid vegetation are described in full in ref. 6, and summarized briefly as follows. Methanol-corrected δD values from fatty-acid methyl esters ($\delta D_{\rm FA}$) were corrected for variations in seawater isotope composition related to global ice-volume variations during the deglaciation using a record of global relative sea-level changes⁵¹ to infer variations in the oxygen-isotope composition of sea water ($\delta^{18}O_{SW}$) related to variations in global ice volume across the deglaciation. Relative sea-level variations were converted to variations in $\delta^{18}O_{\text{SW}}$ using a scaling factor of 1.0% per 127.5 m of relative sea-level change 52 . Variations in $\delta^{18}O_{SW}$ were subsequently converted to variations in δD_{SW} using the slope of the global meteoric water line. Finally, ice-volume-corrected FAMES δD values ($\delta D_{\text{FA-IV}}$) were calculated by correcting measured δD_{FA} for changes in δD_{SW} relative to the modern seawater composition. $\delta D_{\text{FA-IV}}$ values were then corrected for variable D/H fractionation by each of C3 and C4 vegetation endmembers to estimate precipitation δD values (δD_P) . Estimated D/H fractionation factors (ϵ) of -125% (100% C3 trees vegetation; ε_{C3}) and -145% (100% C4 grasses vegetation; ε_{C4}) were applied on the basis of variable C3 and C4 mixing proportions determined from sample FAMES δ^{13} C values following ref. ⁵³.

Constraining soil carbon fluxes

Under steady-state conditions, the soil carbon turnover time (T_r) can be given as a function of the total mass of soil carbon (M_s) and soil carbon inputs (NPP (F_p)) and outputs (F_{out}) , where F_{out} is a combination of fluxes from heterotrophic respiration (F_r) , fire emissions (F_t) and river erosion and export (lateral fluxes, F_t) as follows:

$$T_{\rm r} = \frac{M_{\rm s}}{F_{\rm p}} = \frac{M_{\rm s}}{F_{\rm r} + F_{\rm f} + F_{\rm l}} \tag{1}$$

We first assume that, since the Last Glacial, $F_{\rm out}$ responds only to changes in $F_{\rm r}$ and $F_{\rm l}$. Following the Last Glacial, and through the HCO, climate in the Ganges–Brahmaputra basin gradually becomes wetter, and vegetation trends towards greater dominance by C_3 forests, as opposed to C_4 savanna⁶. Together, these would be far more likely to decrease, as opposed to increase, fire intensity, and thus fire carbon emissions. Thus, holding $F_{\rm f}$ constant presents a conservative estimate of changes in $M_{\rm s}$ and/or $F_{\rm r}$ and $F_{\rm l}$ between the Last Glacial and post-HS1 periods. We also assume that $F_{\rm r}$ and $F_{\rm l}$ remain at their present relative proportions of 97% and 3%, respectively, of the non- $F_{\rm f}$ portion of $F_{\rm out}$. Finally, we assume that soil (millennial) carbon always composes 80% of total carbon burial (see text for details) and that carbon burial efficiency (sediment-volume and grain-size-normalized

burial rates) have remained near 100% since the Last Glacial (discussed in ref. 6).

Our bulk organic-carbon radiocarbon results indicate that the reservoir-age offset (proxy for T_r) of millennial (soil) BOC pools decreased by around 3,800 ¹⁴C years (approximately 56%) between HS1 and the HCO (Supplementary Table 2). Although changing either $F_{\rm p}$ or $F_{\rm out}$ would affect the steady-state turnover time (as per equation (1)), it has no immediate impact on the average age of soil organic carbon, and thus the average BOC reservoir offset value. Thus, observed post-Last Glacial shifts in laterally fluxed BOC are best explained by changes in Ganges-Brahmaputra soil carbon stocks over this time (that is, time-varying M_s). For example, holding F_p and F_{out} constant, we would expect that M_s would vary between approximately 33.2 Pg C at HS1, to roughly 14.4 Pg C at the HCO (a depletion of soil carbon stocks of roughly 56%), and to its modern documented value of 19.52 Pg C (see ref. 4). Likewise, between HS1 and the post-Bølling-Allerød millennial organic-carbon reservoir offset minimum (around 2,500 ¹⁴C years), basin-wide carbon stocks decreased by an amount (about 20.9 Pg) nearly equivalent to the modern basin-wide storage.

Given that BOC delivered to the coastal ocean represents only around 3% of total annual soil-carbon turnover within the Ganges–Brahmaputra basin (about 0.0036 Pg yr $^{-1}$; refs. 23,49), the HS1 to post-Bølling–Allerød decrease in basin-wide soil carbon stocks, if driven entirely by changes in river carbon export, would require lateral fluxes to nearly double for this roughly 3,000-year period. By contrast, a mere 7.5% increase in heterotropic respiration rates would be required to account for the observed decrease in soil carbon stocks between HS1 and the Bølling–Allerød.

Constraining impacts of soil carbon provenance

Changes in the age structure of BOC laterally exported from the Ganges-Brahmaputra rivers cannot be explained by sediment-source variability from within-basin soil profiles (for example, because of erosion of deeper, older carbon during cooler and drier periods, potentially in response to reduced vegetation cover). Since deglaciation, sediments exported by the Ganges-Brahmaputra rivers have become gradually more chemically weathered 6,50 , whereas the BOC exported with these same sediments has become younger; thus, sediment 'age' (as given by pre-export weathering) and BOC age structures are decoupled. Changes in BOC age structure also cannot be explained by changes in sediment provenance from within the basin (for example, by shifting foci of monsoon precipitation associated with changes in monsoon strength⁶). Whereas sediment may be sourced from throughout the Ganges-Brahmaputra basin, BOC delivered to the Bengal Fan is predominantly floodplain in origin, as upland organic carbon is subject to efficient degradation and replacement during transit⁵⁴. BOC age structures should thus be insensitive to sediment sourcing upstream of the floodplain.

Data availability

All new data produced for this study are from samples from Bengal Fan cores SO93-117KL, -118KL and -120KL. These are available in Supplementary Tables and online in the EarthChem Library (http://www.earthchem.org/). Specifically, these present a compilation of radiocarbon age-dating results from planktonic foraminifera used in derivation of core age-depth models (Supplementary Table 1 and https://doi.org/10.1594/IEDA/111486); results of radiocarbon analyses of bulk organic carbon and calculated reservoir offset and F¹⁴R values of bulk and millennial BOC (Supplementary Table 2 and https://doi.org/10.1594/IEDA/111487); results of radiocarbon analyses of fatty-acid homologues and associated calculated reservoir offset and F¹⁴R values of bulk homologues and the subset of those cycled on millennial

timescales (Supplementary Table 3 and https://doi.org/10.1594/IEDA/111488); and abundances of fatty-acid homologues (Supplementary Table 4 and https://doi.org/10.1594/IEDA/111489). Source data for Figs. 1, 2 and Extended Data Figs. 2–7 are provided with the paper.

- Weber, M. E., Wiedicke, M. H., Kudrass, H. R., Hübscher, C. & Erlenkeuser, H. Active growth
 of the Bengal Fan during sea-level rise and highstand. Geology 25, 315–318 (1997).
- Bronk Ramsey, C. B. Bayesian analysis of radiocarbon dates. Radiocarbon 51, 337–360 (2009).
- Reimer, P. J. et al. IntCal13 and Marine13 radiocarbon age calibration curves 0–50,000 years cal BP. Radiocarbon 55, 1869–1887 (2013).
- Dutta, K., Bhushan, R. & Somayajulu, B. ΔR correction values for the northern Indian Ocean. Radiocarbon 43, 483–488 (2001).
- Southon, J., Kashgarian, M., Fontugne, M., Metivier, B. & Yim, W. W. Marine reservoir corrections for the Indian Ocean and Southeast Asia. Radiocarbon 44, 167–180 (2002).
- Blaauw, M. Methods and code for 'classical' age-modelling of radiocarbon sequences. Quat. Geochronol. 5, 512–518 (2010).
- Christl, M. et al. The ETH Zurich AMS facilities: performance parameters and reference materials. Nucl. Instrum. Methods Phys. Res. B 294, 29–38 (2013).
- Eglinton, T. I. et al. Gas chromatographic isolation of individual compounds from complex matrices for radiocarbon dating. Anal. Chem. 68, 904–912 (1996).
- Santos, G. M. et al. Blank assessment for ultra-small radiocarbon samples: chemical extraction and separation versus AMS. *Radiocarbon* 52, 1322–1335 (2010).
- 41. Shah Walter, S. R. et al. Ultra-small graphitization reactors for ultra-microscale ¹⁴C analysis at the National Ocean Sciences Accelerator Mass Spectrometry (NOSAMS) facility.
- Radiocarbon 57, 109–122 (2015).
 Kusch, S., Rethemeyer, J., Schefuß, E. & Mollenhauer, G. Controls on the age of vascular plant biomarkers in Black Sea sediments. Geochim. Cosmochim. Acta 74, 7031–7047 (2010).
- 43. Ohkouchi, N., Eglinton, T. I. & Hayes, J. M. Radiocarbon dating of individual fatty acids as a tool for refining Antarctic margin sediment chronologies. *Radiocarbon* **45**, 17-24 (2003).
- Olsson, I. U. (ed). Radiocarbon Variations and Absolute Chronology: Nobel Symposium, 12th Proc. (John Wilev. 1970).
- Stuiver, M. & Polach, H. A. Discussion: reporting of ¹⁴C data. Radiocarbon 19, 355–363 (1977).
- Reimer, P. J., Brown, T. A. & Reimer, R. W. Discussion: reporting and calibration of post-bomb ¹⁴C data. *Radiocarbon* 46, 1299–1304 (2004).
- Soulet, G. Methods and codes for reservoir-atmosphere [™]C age offset calculations. Quat. Geochronol. 29, 97-103 (2015).
- Galy, V., Beyssac, O., France-Lanord, C. & Eglinton, T. I. Recycling of graphite during Himalayan erosion: a geological stabilization of carbon in the crust. Science 322, 943– 117 (2002).
- Galy, V., Hein, C., France-Lanord, C. & Eglinton, T. in Biogeochemical Dynamics at Major River-Coastal Interfaces: Linkages with Global Change (eds Bianchi, T., Allison, M. & Cai, W.-J.) 353–372 (Cambridge Univ. Press, 2014).
- Lupker, M., France-Lanord, C., Galy, V., Lavé, J. & Kudrass, H. Increasing chemical weathering in the Himalayan system since the Last Glacial Maximum. Earth Planet. Sci. Lett. 365, 243–252 (2013).
- Lambeck, K. & Chappell, J. Sea-level change through the last glacial cycle. Science 292, 679–686 (2001)
- 52. Clark, P. U. et al. The last glacial maximum. Science **325**, 710–714 (2009).
- Collins, J. A. et al. Estimating the hydrogen isotopic composition of past precipitation using leaf-waxes from western Africa. Quat. Sci. Rev. 65, 88-101 (2013).
- Galy, V., Eglinton, T., France-Lanord, C. & Sylva, S. The provenance of vegetation and environmental signatures encoded in vascular plant biomarkers carried by the Ganges– Brahmaputra rivers. Earth Planet. Sci. Lett. 304, 1–12 (2011).
- Schwenk, T., Spieß, V., Hübscher, C. & Breitzke, M. Frequent channel avulsions within the active channel-levee system of the middle Bengal Fan—an exceptional channel-levee development derived from Parasound and Hydrosweep data. Deep Sea Res. Part II Top. Stud. Oceanogr. 50, 1023–1045 (2003).

Acknowledgements We thank C. Johnson (Woods Hole Oceanographic Institution, WHOI) and D. Montluçon (ETH Zürich) for laboratory support. We thank H. Kudrass for assistance with core sampling. This work was supported by a WHOI Coastal Ocean Institute Postdoctoral Fellowship to C.J.H., and by the National Science Foundation (grant numbers OCE-1333826, OCE-1333387 and OCE-1657771). This is contribution number 3868 of the Virginia Institute of Marine Science.

Author contributions C.J.H. and V.V.G. designed the study. C.J.H. conducted laboratory analyses with substantial contributions from V.V.G.; most radiocarbon analyses were conducted by M.U. and N.H. at the Laboratory for Ion Beam Physics (ETH). C.J.H. and V.V.G. drafted the manuscript with contributions from T.I.E.

Competing interests The authors declare no competing interests.

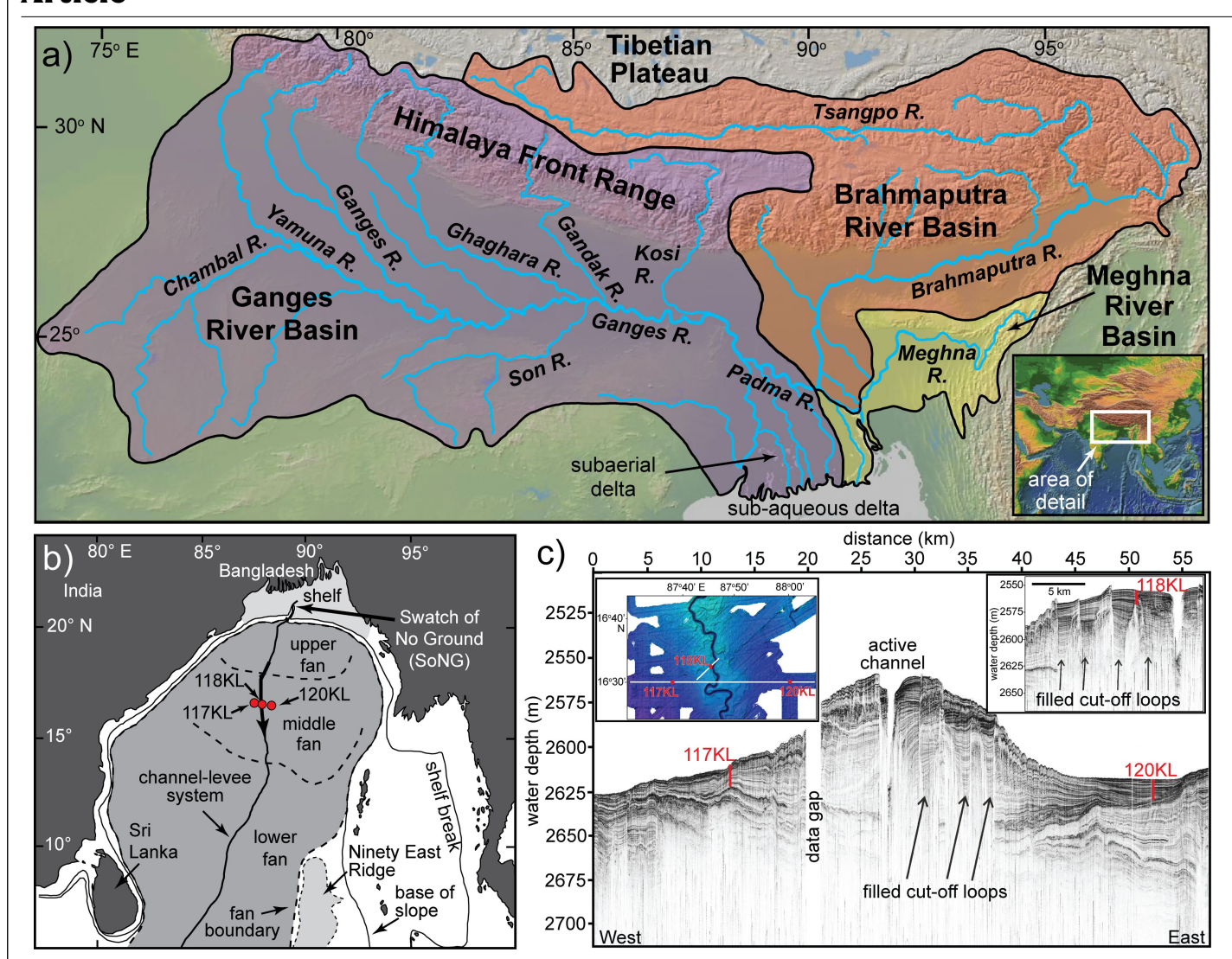
Additional information

Supplementary information is available for this paper at https://doi.org/10.1038/s41586-020-2233-9.

Correspondence and requests for materials should be addressed to C.J.H.

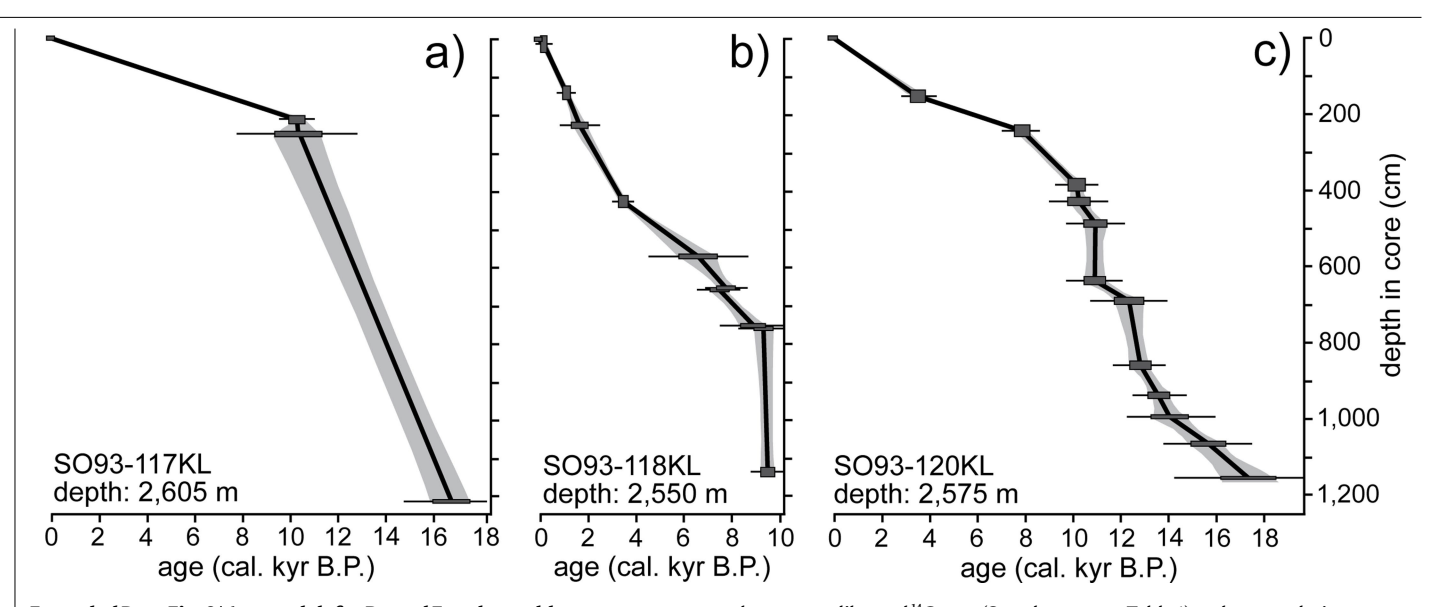
Peer review information Nature thanks Katherine Freeman, Sanjeev Gupta, Yongsong Huang
and the other, anonymous, reviewer(s) for their contribution to the peer review of this work.

Reprints and permissions information is available at http://www.nature.com/reprints.



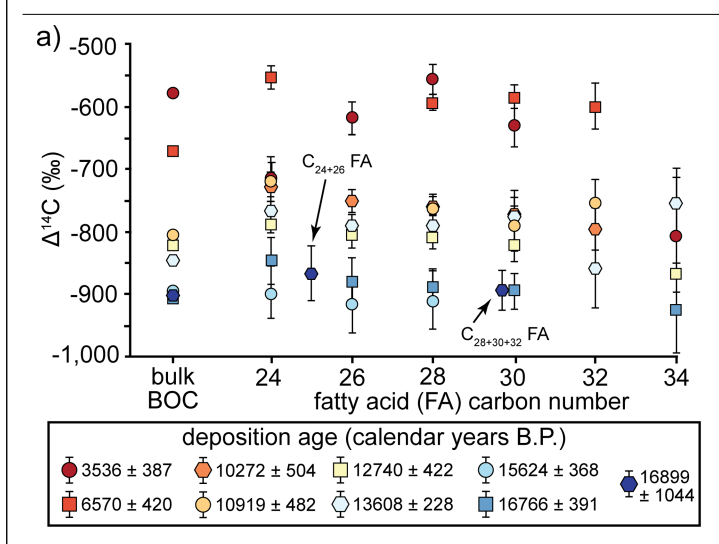
Extended Data Fig. 1 | Study area and data collection. a, Major features and tributaries of the Ganges–Brahmaputra drainage basin. The background topographic image is from GeoMapApp (http://www.geomapapp.org). **b**, Morphology of the Bengal Fan. Sediment is dominantly delivered via turbidity currents that travel along the single-channel channel-levee system. Red circles show sediment cores used here. **c**, A Parasound seismic-reflection

profile crossing cores SO93-117KL and SO93-120KL from west to east. The upper left inset shows locations of the profile and cores with respect to the pathway of the active channel, imaged by multibeam bathymetry. The upper right inset shows Parasound data around core SO93-118 KL. Figure parts are modified from ref. 6, and details of the sediment fan system are described in ref. 55.

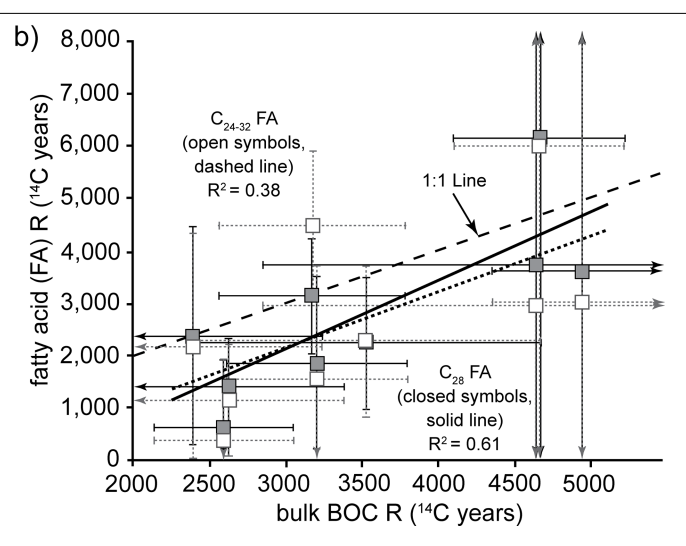


Extended Data Fig. 2 | **Age models for Bengal Fan channel-levee cores. a–c**, Age models for cores SO93-117KL (**a**; number of dated samples, n = 3), SO93-118KL (**b**; n = 10) and SO93-120KL (**c**; n = 12, derived through interpolation

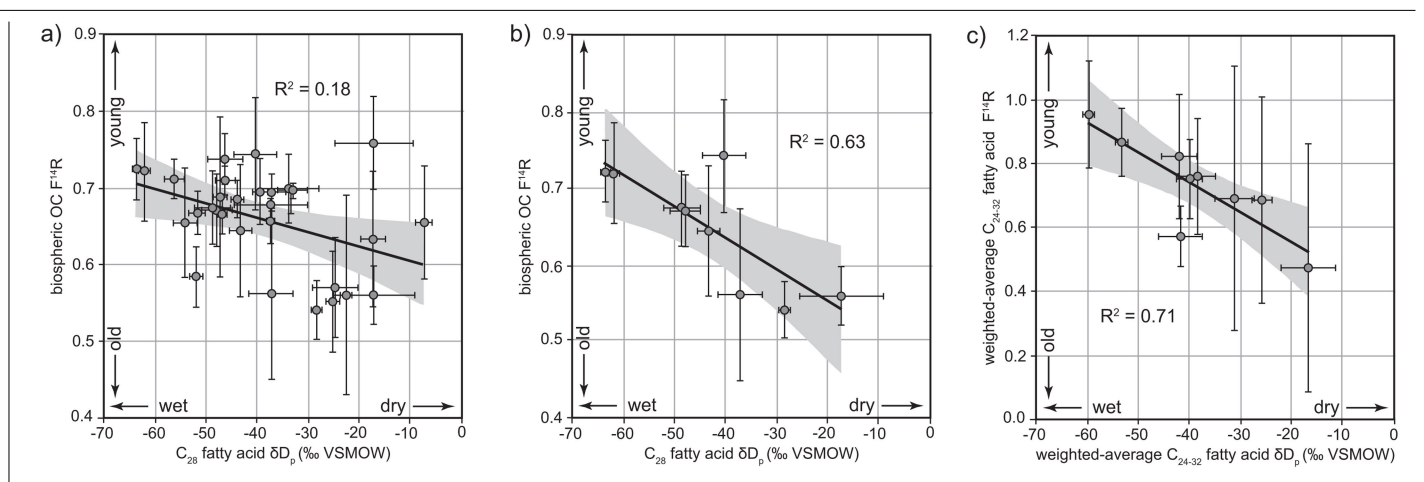
between calibrated ^{14}C ages (Supplementary Table 1) and extrapolation to core tops and bottoms. Box widths represent sample depth intervals within cores; box heights represent calibrated age errors. Figure updated from ref. 6 .



Extended Data Fig. 3 | **Summary of bulk BOC and biomarker (long-chain fatty acid) analyses. a**, Radioisotopic compositions of bulk BOC and individual fatty-acid (FA) homologues (n = 47). Vertical error bars indicate propagated measurement uncertainties. **b**, Comparison between reservoir-age offset (as given by the difference between organic-matter and

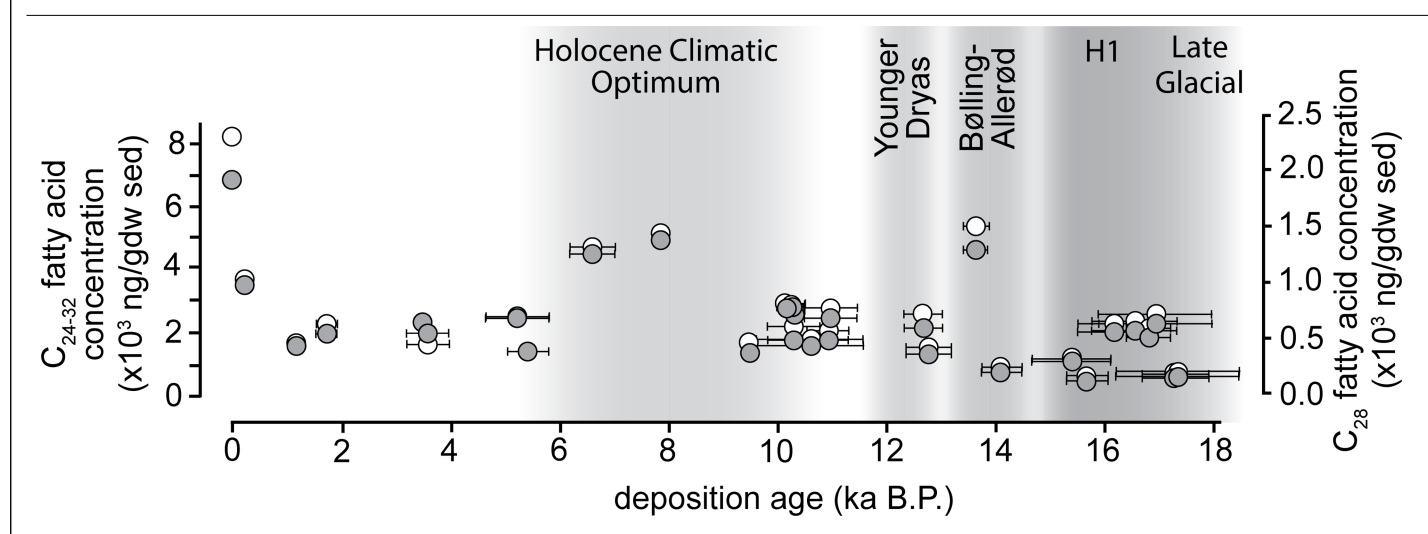


deposition age, in 14 C years) of bulk BOC and C $_{28}$ plus C $_{24-32}$ fatty acids (n=9). Most values fall below the 1:1 line, reflecting the contribution of excess pre-aged organic matter to the bulk BOC pool. Error bars indicate propagated radiocarbon measurement and instrument-correction uncertainties.



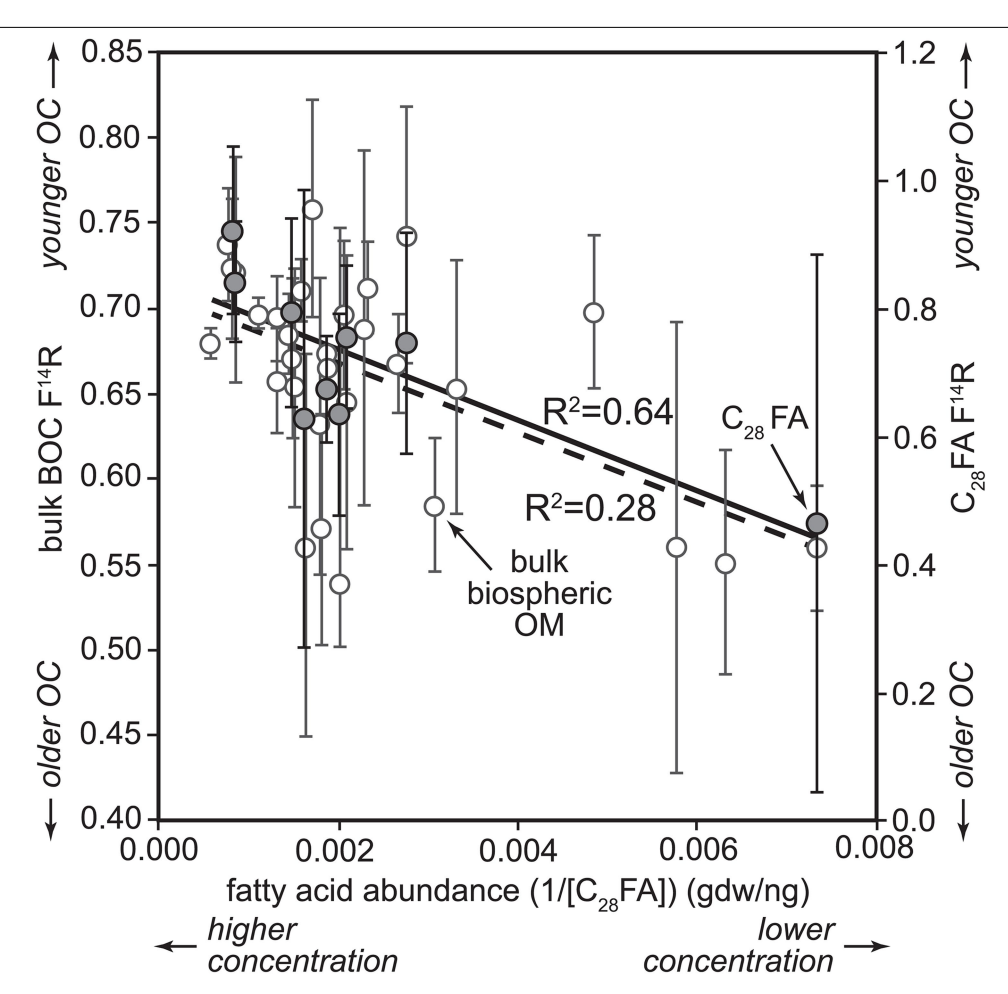
Extended Data Fig. 4 | Correlation between palaeoclimate proxies with organic-matter age structure. a–c, Graphs show comparisons of post-glacial precipitation δD_P values derived from ice-volume- and vegetation-fractionation-corrected fatty-acid δD values (more-depleted values are indicative of a stronger ISM) and the pre-ageing of organic matter (given as F¹⁴R values, in dimensionless Fm units; higher values indicate less pre-ageing). Comparisons shown are: a, bulk BOC versus δD_P of C_{28} fatty acids (n=30) for the comprehensive data set presented

in Supplementary Table 2; **b**, bulk BOC versus $\delta D_{\rm P}$ of C_{28} fatty acids (n=9) for the subset of samples for which we also have compound-specific (fatty-acid) 14 C data (Supplementary Table 3); and **c**, weighted-average F^{14} R values of C_{24-32} fatty acid homologues versus weighted-average $\delta D_{\rm P}$ values of those same C_{24-32} fatty acids (n=9). Vertical error bars indicate propagated radiocarbon measurement and instrument-correction uncertainties; horizontal error bars are propagated multimeasurement standard deviation (δD) errors (see ref. 6). OC, organic carbon.



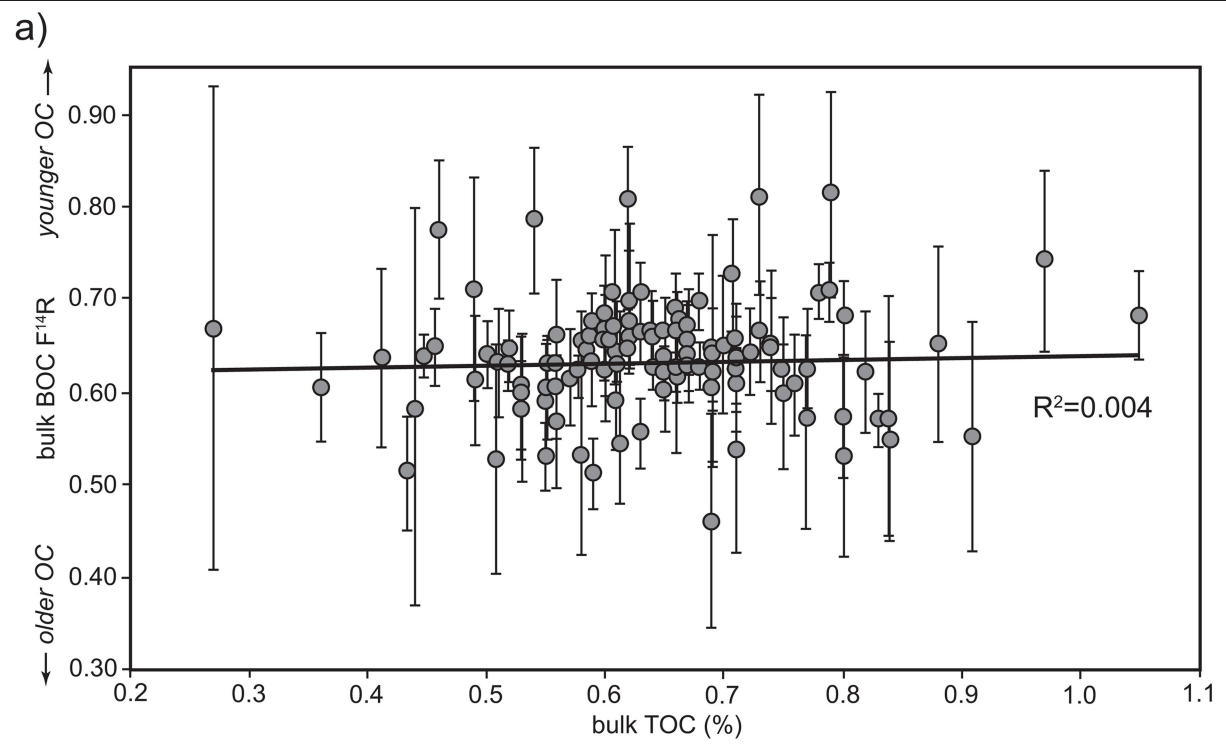
Extended Data Fig. 5 | **Temporal records of fatty-acid abundance in Bengal Fan core sediments.** Abundance of C_{28} (closed circles) and C_{24-32} (open circles) fatty-acid homologues (n=30) in sediments within Bengal Fan channel-levee

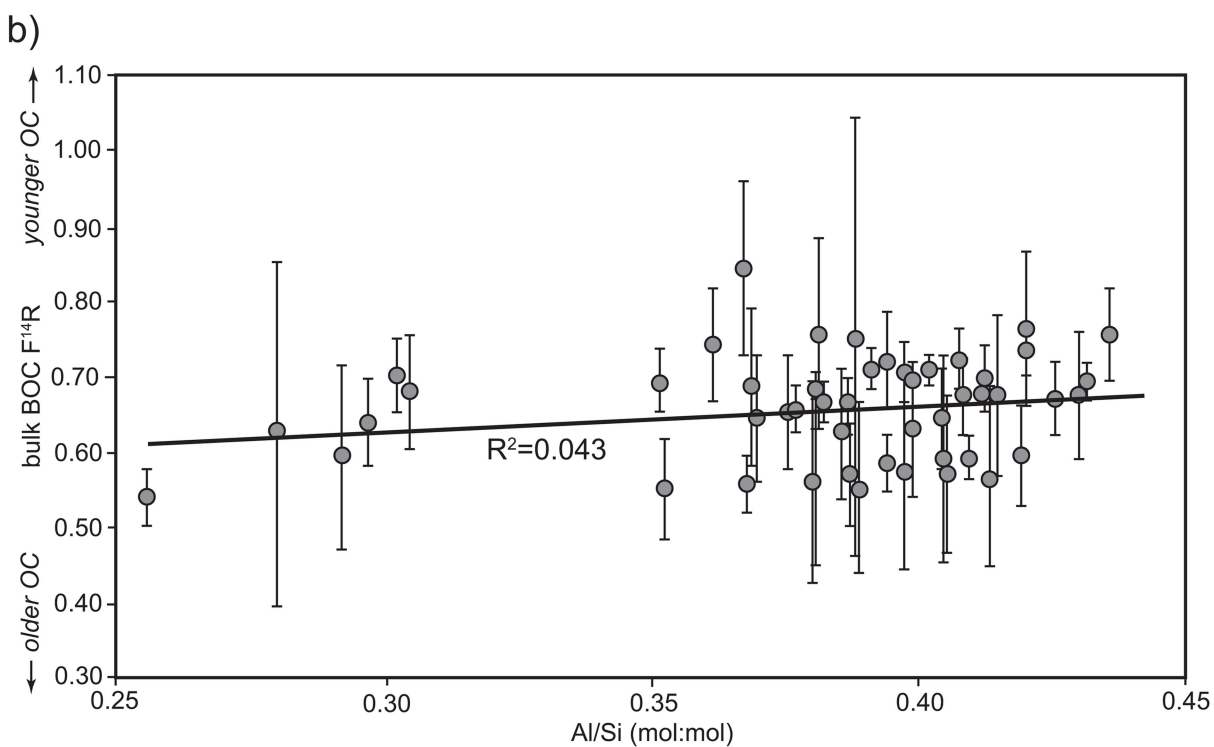
cores since the Late Glacial (data given in Supplementary Table 4). Horizontal error bars represent depositional age uncertainties (from core-age models) and are within data points if not shown.



 $\label{eq:continuous} \textbf{Extended Data Fig. 6} \ | \ \textbf{Correlation between fatty-acid abundance and} \\ \textbf{organic-matter age structure.} \ C_{28} \ \text{fatty-acid abundances} \ (Supplementary Table 4) \ are plotted against F ^{14}R values of bulk BOC (open circles, dashed line; \\ \textbf{Correlation} \ \textbf{Correlation} \$

n = 30) and of C₂₈ fatty acids (closed circles, solid line; n = 9). Vertical error bars indicate propagated radiocarbon measurement and instrument-correction uncertainties.





Extended Data Fig. 7 | Correlation between organic-matter age structure and proxies for sediment and organic-matter composition. a, b, Bulk BOC $F^{14}R$ values are plotted against: a, bulk sediment TOC values, and b, sediment Al/Si values, for all samples used herein for which both data sets exist (n = 116

and n = 50, respectively). Al/Si values in **b** are from refs. ^{6,50}. Vertical error bars indicate propagated radiocarbon measurement and instrument-correction uncertainties.